
Volume 275, Issues 3–4
15 November 2008
ISSN 0012-821X
ELSEVIER
EARTH
& PLANETARY
SCIENCE LETTERS
Editors
Rick Carlson, Washington, DC
Peggy Delaney, Santa Cruz, CA
Peter B. deMenocal, Palisades, NY
T. Mark Harrison, Los Angeles, CA
Tilman Spohn, Berlin
Lars Stixrude, London
Rob van der Hilst, Cambridge, MA
Frontiers Editor
Albrecht W. Hofmann, Mainz

Earth and Planetary Science Letters 275 (2008) 370–381

Contents lists available at ScienceDirect

Earth and Planetary Science Letters

journal homepage: www.elsevier.com/locate/epsl

Small and large-amplitude gravitational instability of an elastically compressible viscoelastic Maxwell solid overlying an inviscid incompressible fluid: Dependence of growth rates on wave number and elastic constants at low Deborah numbers

E.B. Burov [a,*], P. Molnar [b]

[a] Laboratoire de Tectonique UMR 7072, University of Paris VI, Paris, France
[b] Department of Geological Sciences and Cooperative Institute for Research in Environmental Sciences, University of Colorado, Boulder, Colorado 80309-0399, United States

ARTICLE INFO

Article history:
Received 6 April 2007
Received in revised form 12 March 2008
Accepted 26 August 2008
Available online 15 October 2008

Editor: C.P. Jaupart

Keywords:
rheology
visco-elasticity
gravitational instability
mechanics of lithosphere

ABSTRACT

To understand how elasticity affects convective instability of viscoelastic fluids near the viscous limit, we carried out numerical experiments of Rayleigh–Taylor instability of compressible viscoelastic fluids overlying inviscid inelastic substrata (hence with infinite viscosity and elasticity ratios). Unlike incompressible viscous fluids, for which growth becomes super-exponential when perturbations to the thickness of the unstable layer grow to several tens of percent of the thickness, for compressible viscoelastic fluids, super-exponential growth does not appear to develop at relatively low Deborah numbers, $De = \Delta\rho g h/\eta \sim 10^{-6}$–$10^{-4}$ (where $\Delta\rho$ is the density difference between unstable layer and substratum, g is gravity, h is the thickness of the unstable layer, and η is its viscosity) and for very high ($>10^6$) ratios of viscosity between layer and substratum, which characterize large-scale geodynamic systems. This behavior differs from that of viscoelastic two-layer systems with higher Deborah numbers ($>10^{-4}$) and with smaller viscosity ratios ($<10^4$) because, instead of accelerating the instability, as for incompressible media, elastic deformation may also retard growth in its most rapid phase as the amplitude of flow increases. For small De ($<10^{-3}$–10^{-4}), retardation of growth manifests itself in three ways: (1) while perturbations remain small, the commonly observed exponential growth is delayed, (2) during exponential growth, the growth rate decreases monotonically with decreasing De, and (3) when perturbations grow to large amplitude ($>100\%$), the exponential growth rate decreases, due to the formation of a compressible viscoelastic drop that has a distinguishable drop head and a stretched filament. Values of De appropriate for Earth's mantle suggest that in most circumstances elasticity will not affect the growth of lithospheric instabilities, but for high density contrasts (e.g. atypically warm lithosphere) elasticity may retard their growth. By contrast, for relatively large Deborah numbers ($>10^{-3}$), finite viscosity ratios ($<10^7$), and small amplitudes of perturbations, elasticity accelerates growth of the instability.

1. Introduction

The steep temperature gradient across the lithosphere makes its lower part, if not the entire mantle lithosphere, convectively unstable. The degree to which growth of unstable perturbations to the thickness or density structure of the lithosphere manifest themselves in geologically observed phenomena remains controversial, but recent studies suggest that the mantle lithosphere, including layers of eclogitic lower crust, beneath both the Sierra Nevada of California (Ducea and Saleeby, 1996, 1998; Jones et al., 2004) and the Altiplano of the central Andes (Garzione et al., 2006; Ghosh et al., 2006) has been removed in late Cenozoic time, and such a possibility seems likely in other regions. It follows that to understand how lithosphere is removed, we must quantify how boundary conditions and rheological properties of the lithosphere affect growth rates of such an instability, the lateral dimensions or characteristic wavelength of the fastest growing perturbations, and the degree to which only part or all of the mantle lithosphere could be removed. Toward that end, we explored the role that elasticity plays in Rayleigh–Taylor instability.

We are motivated by the idea that convective removal of part or all of the mantle lithosphere could occur in a relatively short time of a few million years (<10 Myr) (e.g., Houseman et al., 1981; Houseman and Molnar, 1997). The characteristic time constant for diffusion of heat into a slab many tens to 100 km thick is tens to hundreds of million years. Thus, diffusion of heat is not likely to affect convective removal at short timescales. This argument justifies analyzing Rayleigh–Taylor instability, instead of full (i.e., Rayleigh–Bénard) convective instability. Indeed, simple scaling arguments derived for Rayleigh–Taylor instability with a variety of rheological conditions (e.g., Houseman and Molnar, 1997) apply well to convective instability (Conrad and Molnar, 1999).

Although we may ignore thermal diffusion, where viscosity is large, the relaxation of elastic stresses in a viscoelastic lithosphere can

* Corresponding author.
E-mail address: evgenii.burov@upmc.fr (E.B. Burov).

0012-821X/$ – see front matter © 2008 Elsevier B.V. All rights reserved.
doi:10.1016/j.epsl.2008.08.032

occur with time scales comparable to that for growth of Rayleigh–Taylor instability of viscous layers. If depth-averaged lithosphere viscosity ranges between 5×10^{19} Pa s to 5×10^{22} Pa s, corresponding average Maxwell or Kelvin–Voigt relaxation times, $t_M=\eta/\mu$, where η is viscosity and $\mu(\cong 7\times 10$ Pa s in the upper mantle) is the shear modulus, are much less than 1 Myr. For more realistic non-Newtonian constitutive laws, however, effective Newtonian viscosities may be as large as 10^{24} Pa s or even higher in the upper, cold levels ($T<1000$ °C) of the mantle. Thus, Maxwell relaxation times can approach 1 Myr, and, in some localized uppermost levels, 10 Myr. Consequently, unlike purely viscous layers, a viscoelastic lithosphere may "feel" previous deformation within geologically appropriate periods of time. This requires consideration of viscoelastic behavior rather than simply viscous behavior.

2. Theory

2.1. General considerations

Stresses in viscoelastic solids (modeled as Maxwell-type solids with viscous and elastic shear components in series) act on three time scales: (1) instantaneous elastic response controlled by the shear and bulk moduli (U, B): (2) relaxation of shear stresses on the timescale controlled by the Maxwell time t_M and (3) creep of the viscous fluid controlled by its dynamic viscosity U. The behavior of such solids is effectively elastic until the incremental elastic strain is reduced to levels smaller than the viscous strain. In the case of increasing strain rate, as occurs during a growing instability, elastic strain may be maintained at high levels that prevent the system from relaxing to pure viscous flow. Brittle strength increases with depth/pressure. Because of that and because of the viscous part of the constitutive law, fracture need not occur at large strains. The development of an instability is regulated by two characteristic times, the Maxwell time defined above, and another that scales the exponential growth of Rayleigh–Taylor instability of a purely viscous layer:

$$t_f = \frac{\eta}{\Delta\rho g h} \tag{1}$$

Here the density of the unstable layer is greater than that in the underlying halfspace by $\Delta\rho$, the thickness of the layer is h, and g is gravity (Table 1). The development of the instability thus depends on the ratio of these two time scales:

$$De = \frac{t_M}{t_f} = \frac{\Delta\rho g h}{\mu} \tag{2}$$

De is a Deborah number, which scales the relaxation time of a fluid process to a characteristic observation time (e.g., Reiner, 1964).

A general theory for viscoelastic Rayleigh–Taylor instability does not seem to exist, in part because quite different behavior can develop for a variety of limiting assumptions for constitutive relationships. Moreover, as for Rayleigh–Taylor instability of a viscous fluid, the temporal development of unstable growth of a viscoelastic fluid changes as the amplitude of the perturbation grows to be comparable and greater than the initial thickness of the unstable layer. Although published theoretical analyses do not address the conditions that we have considered, we review briefly published theories here.

In the general case, solutions of the equilibrium equations for time-dependent deflection, $W(t,x)$, of a viscous or viscoelastic layer are presented as the sum of a damped (stable) part, decaying exponentially with time, and an unstable part, growing exponentially with time (e.g., Biot, 1965a,b; Biot and Odé, 1962, 1965; Odé, 1966; Burov et al., 1993, Appendix: Nadai, 1963). The growth (or decay) rate p depends on the boundary conditions, constitutive relations, wavelength, and geometry of the structure, and $1/p$ either equals or depends on the Maxwell time, t_M (Biot, 1965a,b; Nadai, 1963).

Table 1
List of symbols

B	Bulk modulus
$De=\Delta\rho gh/\eta=t_f/t_M$	Deborah number (dimensionless)
$De_e=De\eta_1/(\eta_2\Delta t')$	Effective Deborah number (for two viscous layers)
E	Young's modulus
g	Gravity (9.8 m s^{-2})
h	Layer thickness
Δh	Amplitude of perturbation to layer interface
$\Delta h'=\Delta h/h$	Dimensionless amplitude of perturbation to layer interface
$k=2\pi/\lambda$	Wavenumber
$k'=kh$	Dimensionless wavenumber
L	Length of filament connecting a sinking drop and overlying layer
$p=\Delta\rho gh/r\,\eta$	Growth rate of instability
P	Pressure (static)
$q'=p\,\Delta\rho gh/\eta$	Dimensionless growth rate of instability
r	Dimensionless growth time factor (see definition of p) that depends on boundary conditions and constitute relationships of layers
t	Time
$t'=t/t_f$	Dimensionless time
$t_f=\eta/\Delta\rho gh$	Time scale for growth of viscous instability
$t_M=\eta/\mu$	Maxwell time
T	Temperature
Δt	Time step in numerical integration
$\Delta t'$	Dimensionless time scale for growth rate of two-layered viscoelastic medium with large De
u	Displacement
w	Rate of vertical movement of layer interface
W	Vertical displacement of layer interface
x	Horizontal position
Z'	Dimensionless depth of maximum descent of perturbation to the layer interface
δ_i	Kronecker delta
δp	Dynamic pressure
ε_{ij}	Strain tensor
$\dot\varepsilon$	Strain rate
η	Dynamic viscosity
η_1	Dynamic viscosity of upper layer
η_2	Dynamic viscosity of substratum
$\eta_{eff}=(\eta_1\eta_2)^{1/2}$	Effective dynamic viscosity for the case of two layers
λ	Wavelength
μ	Shear modulus (3×10^9–3×10^{12} Pa)
ν	Poisson's ratio (0.25)
ρ	Density (3.3×10^3 kg/m^3)
$\Delta\rho$	Density difference between layer and substratum
σ_{ij}	Stress tensor
$\sigma_{Maxwell}$	Maxwell stress (product of effective viscosity and strain rate)
τ_{ij}	Deviatoric tress tensor
ω_{ij}	Rotation tensor
ψ	Stream function

For layered incompressible media with a finite, but not very large, viscosity contrast between layers (viscosity ratios $<10^2$) and with no contrast in elastic moduli, Biot (1965a,b), Biot and Odé (1962) and Odé (1966) showed that small elastic shear moduli result in higher growth rates of Rayleigh–Taylor instability than for larger shear moduli (see also Appendix):

$$p = \frac{\Delta\rho g h}{\eta r} = \frac{De}{r t_M} \tag{3a}$$

Here, $r>0$ is a non-dimensional scaling (it refers to a positive root of the characteristic stability equation, Appendix A) that depends on the boundary conditions and the wavelength of the perturbation. Biot (1965b) suggested that for a limited viscosity contrast between the layer (η_1) and substratum (η_2) and when vertical deflection of the layer interface is small, the viscosity η can be replaced by the effective viscosity $\eta_{eff}=(\eta_1\eta_2)^{1/2}$. Poliakov et al. (1993) showed that for a viscoelastic media with no contrast in elastic moduli or viscosity, the growth rate factor can be also written as:

$$p = \frac{\Delta\rho g h}{\eta\left(r - \frac{\Delta\rho g h}{\mu}\right)} = \frac{\Delta\rho g h}{\eta(r - De)} \tag{3b}$$

It follows that a decrease in the shear modulus μ results in a higher growth rate compared to a purely viscous case with the same viscosity η, for $0<De<r$. For the earth, however, as we show below, $De \ll 1$ (typically $De<10^{-3}$, and elasticity would sensibly increase the growth rate only for $r \ll 1$. In most cases considered by Biot (1965a,b), r is on the order of 1. Also, obviously, Eq. (3b) fails when the shear modulus becomes $\le \Delta\rho g h$ ($De \ge 1$) as p becomes infinite when $De=1$. This is also physically impossible due the fact that Frenkel's limit prohibits $De>0.1$–0.2 (e.g., Kittel, 1986).

Faster growth of the instability for small elastic moduli can be understood as follows. For a fixed strain increment, the smaller is shear modulus, the smaller is the elastic restoring force. Because Maxwell elastic and viscous shear stresses are equal, low elastic moduli imply lower stresses for the same strain increments and the same strain rates. Thus, the small elastic moduli lead to an effectively weaker material. From the perspective of the viscous response of the medium, a smaller elastic modulus calls for a smaller effective viscosity η_{app}, $\eta_{app}=\tau\,\dot{\varepsilon}=\sigma_{Maxwell}/\dot{\varepsilon}$, compared to the intrinsic viscosity, η, where $\sigma_{Maxwell}$ is the Maxwell shear stress. For a given perturbation to the base of an unstable layer, growth will be faster when the effective viscosity is lower. It must be also noted that although decreasing the shear modulus decreases the effective viscosity of the layer, it also increases the relaxation time $t_M=\eta/\mu$. The first effect reduces time scale for the effectively viscous instability, but the second effect increases the time scale for the instability to develop, as we show below.

Poliakov et al. (1993) numerically validated Biot's (1965a,b), Biot and Odé's (1962) and Odé's (1966) predictions for the cases of two fluids with finite viscosity contrast ($<10^4$), zero elasticity contrast, $De>10^{-4}$, and for perturbations with amplitudes on the order of h. Kaus and Becker (2007) repeated and extended the numerical experiments of Poliakov et al. (1993) to confirm their applicability for large values of viscosity ($\eta>10^{21}$ Pa s) and large Deborah numbers ($De>10^2$), as well as for the cases when the lower layer is purely viscous (elastic moduli in the lower layer are infinite).

Kaus and Becker (2007) offered a semi-analytical solution for the case of a viscoelastic fluid (η_1) over a viscous fluid (η_2), based on the assumption of the applicability of an "apparent" viscosity $\eta_{\mathrm{app}}=\frac{\dot{\varepsilon}^{\mathrm{vis}}}{\dot{\varepsilon}}\frac{\eta_1}{\eta_2}$ and an apparent Deborah number, $De_{\mathrm{e}}=De\,\eta_1/(\eta_2\Delta t')$, where $\Delta t'$ is a dimensionless time interval. Although they carried out elegant analysis of this problem, we think that this approximation is of limited value for lithospheric dynamics. Frenkel's limit (e.g., Kittel, 1986) on the strength of the atomic bonds requires that $\Delta\rho g h$ be less than approximately 0.25 μ. Consequently, for tectonically relevant $\Delta\rho g h$ on the order 100 MPa, De must be less than 4×10^8Pa s μ^{-1}.

For example, for $\mu=30$ GPa, $De<0.01$. Kaus and Becker's analysis, however, applies to cases with $De>10^{-2}$, as they show with numerical experiments.

Poliakov et al. (1993) showed that for fluids with same elastic moduli, the behavior is nearly viscous for an "effective" $De_{\mathrm{e}} \ll 1$ and for $\eta_1/\eta_2<10^2$, and nearly elastic for $De_{\mathrm{e}} \gg 1$ and $\eta_1/\eta_2>10^4$. They did not investigate cases $De_{\mathrm{e}} \ll 1$ and $\eta_1/\eta_2>10^4$ or $De_{\mathrm{e}} \gg 1$ and $\eta_1/\eta_2<10^2$. Poliakov et al. (1993) concluded that for a fixed value of De_{e}, the growth rate of the instability decreases with increasing η_1/η_2 or with decreasing De_{e}. This result is controversial, however, because for an infinite viscosity ratio $De_{\mathrm{e}} \to \infty$, which, according to Biot's theory, implies that the system should behave elastically and grow fastest. Indeed, for a finite viscosity contrast, with a viscoelastic fluid overlying a viscous fluid, Kaus and Becker (2007) found that the growth rate increases with increasing viscosity ratio. The case with $De_{\mathrm{e}} \to \infty$ thus presents a particular situation, because the effective Deborah number De_{e} does not directly depend on De, and thus on the elastic properties, but variation of De may indirectly influence on the growth rate.

Finally, but importantly, Poliakov et al. (1993) have indicated that elastic compressibility may also have an important effect on the growth rate of instabilities by demonstrating that the accelerating effect of elasticity increases with decreasing Poisson's ratio.

In summary, depending on the elastic and viscous structure of the medium, elastic deformation can either accelerate or delay the growth of Rayleigh–Taylor instability. For small values of De appropriate for the lithosphere–asthenosphere system, however, finite elasticity seems unlikely to accelerate growth, and our goal is to examine quantitatively how elasticity does affect such growth.

2.2. Compressibility and large-amplitude viscoelastic drop theory

For large vertical deflections ($W>h$), Biot's theory does not apply, and the problem of gravitational instabilities in layered media becomes that for a viscoelastic drop (or diapir in the case of an inverted structure) and its filament translating through a viscous (e.g., Whitehead and Luther, 1975) or viscoelastic environment (e.g., Bird et al., 1987) (Fig. 1A). Indeed, in real fluids, as the amplitude of the perturbation grows to approximately one layer thickness, the slope of the bottom of the deflected layer may increase to become subvertical, and a drop head forms (Fig. 1A). At micro-scales, the development of viscous drops is largely controlled by surface tension, which may cause the instability to stall, but is of no importance at the macro-scale. Yet, in case of viscoelastic fluids, tensional stresses and buoyancy forces at the surface of the drop contribute to a damping of the instability and somehow play a similar role as surface tension (Appendix A, Eqs. (A3), (A5), and (A6)). The drop head is connected to the horizontal source layer by a filament, with length $L>h$, that stretches progressively and becomes thinner than both the source layer and the diameter of the drop head. In this case, the growth rate of the instability is controlled by stretching rate of the filament, which depends on the weight of the drop and the rate of the flow from the source layer that feeds the filament.

A filament can be stretched over many layer thicknesses after the vertical deflection W exceeds the initial layer thickness, h (e.g., Smolka and Belmonte, 2003; Smolka et al., 2004). Unlike that in incompressible Newtonian fluids, downward stretching of a viscoelastic filament results in vertical dilatation and horizontal contraction and creates a dynamic restoring force that must be relaxed before the drop can descend. As result, a viscoelastic drop slows down when the elastic restoring force becomes sufficiently large to compete with the weight of the drop and filament.

In Appendix B, we review briefly an analysis given by Smolka and Belmonte (2003), but here we note an aspect relevant to our work. Compressibility of the viscoelastic fluid can play a key role in finite amplitude growth, because with greater compressibility (relatively small elastic moduli), the diameter of the filament connecting the drop to the remaining fluid can be small, which makes the weight of the drop plus fluid smaller than in incompressible fluids. Thus, during finite amplitude growth, large compressibility and associated less massive drops and filaments will lead to slower growth than for smaller compressibility (larger elastic moduli).

3. Basic equations and assumptions

As shown above, analytical approaches are limited, which justifies a numerical approach. With that goal, we consider the general static equation of equilibrium that conserves momentum:

$$\nabla\cdot\sigma_{ij}-\rho g\delta_i=0 \tag{4a}$$

Here σ_{ij} is the stress tensor, $\rho(x,y,z)$ is density, g is gravity, and δ_i is the Kronecker delta (meant here as a unit vector in vertical direction). In our analysis, the body force (second term) arises from a constant density contrast $\Delta\rho$ between the upper layer (lithosphere) and underlying fluid (asthenosphere). Thus, we may reduce Eq. (4a) to:

$$\nabla\cdot\sigma_{ij}-\Delta\rho g\delta_i=0 \tag{4b}$$

Assuming a negative sign for static pressure, we can present σ_{ij} as:

$$\sigma_{ij}=\tau_{ij}-P+\delta p \tag{5}$$

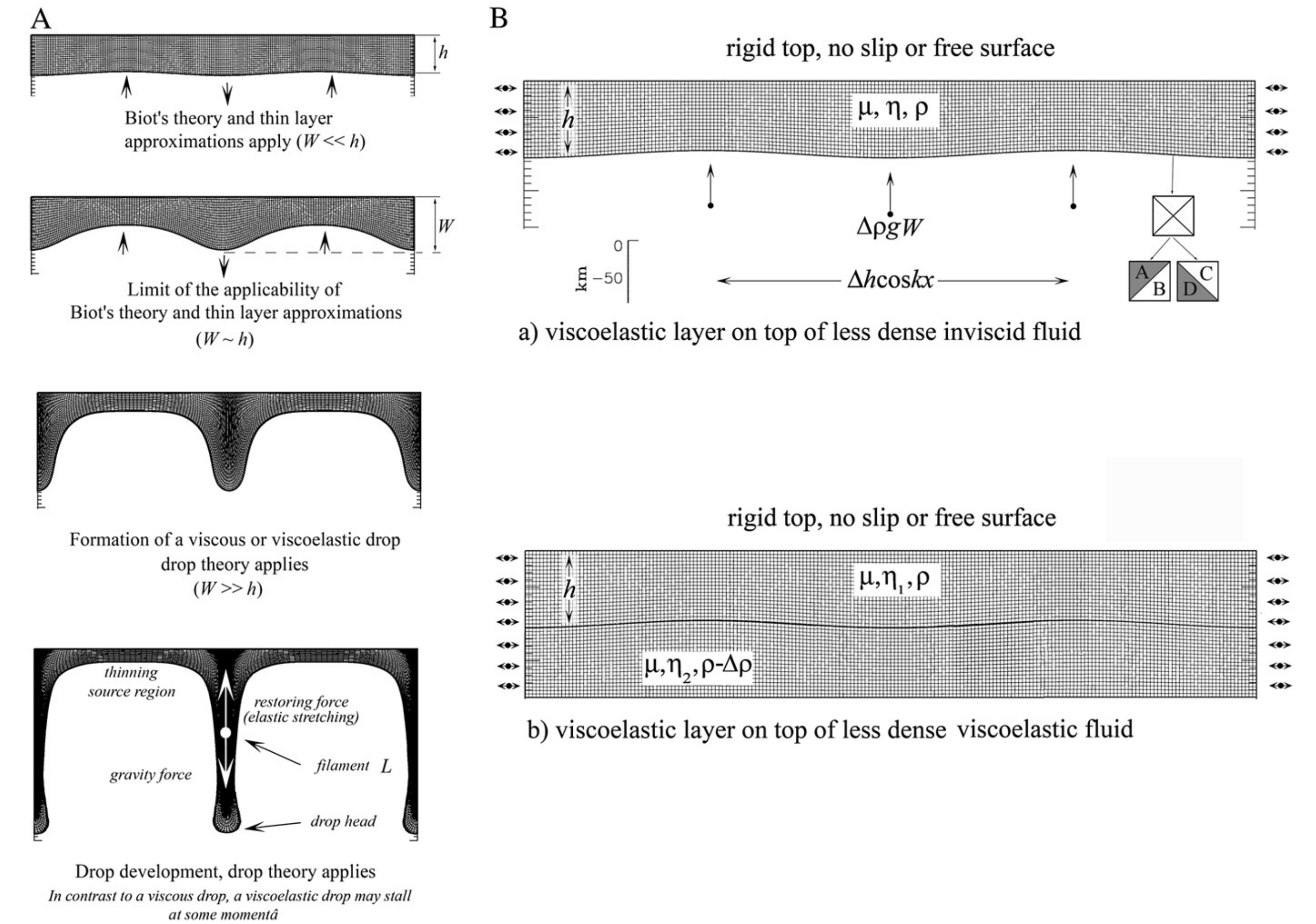

Fig. 1. A) Sequence of different stages of development of a Rayleigh–Taylor instability in a viscoelastic layer of thickness h overlying an inviscid fluid of lower density. (These plots are based on real numerical run, which is used here for illustration only.) When the amplitude W of the instability is small ($W<h$), Biot's linear theory applies. At later stages ($W>h$), Biot's theory is not applicable and drop theory applies. At this moment, the elastic restoring force due to stretching of drop filament starts to play an important role in the development of the instability, and descent of the drop may stall at some point. B) Numerical setup for experiments. Case a): Main setup with a viscoelastic layer on top of inviscid fluid. The initial grid is composed of 200×20 rectangular elements containing 800×80 overlapping sub-triangles that represent a 100-km thick viscoelastic mantle lithosphere layer with elastic shear modulus μ, viscosity η, and density ρ (see insert showing a rectangular element subdivided onto triangles A,B,C,D). The bottom of the lithosphere is initially perturbed with a harmonic perturbation of wavelength λ and amplitude Δh (5 km). The bottom boundary condition is Winkler's hydrostatic condition that simulates an underlying inviscid fluid of density $\rho-\Delta\rho$. At lateral edges, reflecting boundary conditions are imposed. The upper boundary condition was one of a free upper surface (stress free), no vertical slip but free horizontal slip (slippery top), or a rigid top. To consider a range of wavelengths, the width of the box varied from 250 km to 2000 km. Case b): a viscoelastic layer on top of less dense viscoelastic fluid. The second setup was used only for benchmarking previous results of Poliakov et al. (1993).

where τ_{ij} is the deviatoric stress, P is static pressure, which depends on depth, and δp is the dynamic pressure that arises due to deformation.

The relations (1–3) refer to idealized incompressible Maxwell fluids, whereas real rocks are at least elastically compressible (Poisson's ratios ~ 0.25). To approximate viscoelasticity better, we use a linear elastically compressible solid with Maxwell shear term, defined by the following constitutive relationships:

$$\begin{cases} \sigma_{ij} = \tau_{ij} + \sigma^I \delta_{ij} \\ \sigma^I = \dfrac{1}{3}\sigma_{ii} + B\varepsilon_{ii} \\ \tau_{ij} = \sigma_{ij} - \dfrac{1}{3}\sigma_{ij}\delta_{ij} \\ \dfrac{\partial \tau_{ij}}{\partial t} = 2\left(\mu\dot{\varepsilon}^d_{ij} - \dfrac{\tau_{ij}}{2t_M}\right) \end{cases} \tag{6}$$

where ε_{ij} is the strain tensor, "M" means "Maxwell", "d" means deviatoric, B is a finite bulk modulus, σ^I is the isotropic stress, or total pressure, so that the fluid is elastically compressible, and we use the Einstein summation convention for repeated subscripts. The bulk viscosity of lithospheric rocks is considered to be negligibly small, in the absence of experimental data that can prove opposite.

We do not solve Eqs. (4a)–(6) analytically, but instead we use a numerical approach based on the viscoelastic-plastic code FLAC-Para(o)voz (Fast Lagrangian Analysis of Continua) (Cundall, 1989; Poliakov et al., 1993). Para(o)voz employs a hybrid Lagrangian (finite difference-finite volume element) numerical scheme, in which the coordinate frame is Cartesian 2D, but stress/strain relations are computed with a full 3D formulation (see details in Burov and Guillou-Frottier, 2005). The code is based on a large-strain, fully explicit time-marching scheme. Locally it solves the full Newtonian equations of motion in the continuum mechanics approximation Eq. (4a):

$$\begin{cases} \dfrac{\partial \tau_{ij}}{\partial t} = 2\left(\mu\dot{\varepsilon}^d_{ij} - \dfrac{\tau_{ij}}{2t_M}\right) \\ \sigma^I = \dfrac{1}{3}\sigma^{\text{old}}_{ii} + B\varepsilon_{ii} \\ \sigma_{ij} = \sigma^{\text{old}}_{ij} + \dfrac{\partial \tau_{ij}}{\partial t}\Delta t + \dfrac{\partial \sigma^I}{\partial t}\Delta t \\ \omega_{ij} = \dfrac{1}{2}\left\{\dfrac{\partial \cdot u_i}{\partial x_j} - \dfrac{\partial \cdot u_j}{\partial x_i}\right\} \\ \sigma^{\text{corrected}}_{ij} = \sigma_{ij} + \left(\omega_{ik}\sigma_{kj} - \sigma_{ik}\omega_{kj}\right)\Delta t \end{cases} \tag{7}$$

where "old" means stress value from the previous time step, Δt is the time step, "corrected" refers to stress tensor corrected for large strain deformation, u is displacement and overdot means time derivative. Solutions of the equations of motion provide velocities at mesh points used for computation of strains in the elements. These strains are then used in Eq. (6) (or Eq. (7)) to calculate stresses within elements, and the equivalent forces are used to compute increments of displacement (velocities) for the next time step. Para(o)voz uses all components of stress σ_{ij}, which allows for the computation of total pressure σ^{I}. Para(o)voz uses an explicit dynamic scheme. When in quasi-static mode, the inertial terms are artificially damped to accelerate computations, whose criterion is determined by the value of the numerical Reynolds number (ratio of inertial forces to viscous forces) that should be kept below 10^{-2} (Poliakov et al., 1993). This condition was respected during the numerical experiments by automatic adjustment of the time step.

The numerical mesh used in all calculations consists of 200×20 quadrilateral elements (Fig. 1B) containing 200×20×4 overlapping sub-triangles (4 triangles per element) for the upper layer. The use of overlapping triangular elements minimizes meshlocking, and thus artificial overpressure. The reaction of the underlying inviscid substratum of density ($\rho-\Delta\rho$) is reproduced by Winkler's boundary condition: a hydrostatic stress equal to $\Delta\rho g W$, where W is vertical deflection of the bottom of the layer. We used reflecting lateral boundary conditions (zero horizontal velocity and zero normal stress). As discussed below, we carried out experiments with three different boundary conditions for the top surface. To analyze results and to compare with others, we non-dimensionalize (4)–(6) as follows. We scale distances to the thickness of the unstable layer, h:

$$(x, z) = h(x', z') \tag{8a}$$

Although, we might scale time using the Maxwell time, $t_M=\eta/\mu$, instead we use characteristic flow time, which is inverse of Biot's (1965a,b) growth rate factor p_b:

$$t_f = \frac{r}{p_b} = \eta/\Delta\rho g h, \tag{8b}$$

because t_f scales as the growth time for the Rayleigh–Taylor instability of viscous fluids (e.g., Chandrasekhar, 1961) and is commonly used in related problems. Thus, we non-dimensionalize time by:

$$t = t_f t' \tag{8c}$$

Following the same tradition, we scale stresses and pressure by $\Delta\rho g h$:

$$(\sigma_{ij}, \tau_{ij}, \delta p) = \Delta\rho g h(\sigma'_{ij}, \tau'_{ij}, \delta p') \tag{8d}$$

In terms of dimensionless quantities, the governing equations become:

$$\nabla' \cdot \sigma'_{ij} - \delta_j = 0 \tag{9}$$

with

$$\frac{\partial \varepsilon_{ij}}{\partial t'} = \frac{\Delta\rho g h}{2\mu}\frac{\partial \tau'_{ij}}{\partial t'} + \frac{\tau'_{ij}}{2} = \frac{1}{2}\left(De\frac{\partial \tau'_{ij}}{\partial t'} + \tau'_{ij}\right) \tag{10}$$

where the dimensionless Deborah number, De, is defined in Eq. (2).

Finally, we write for the dilatation:

$$\varepsilon_{ii} = \frac{\Delta\rho g h}{B}\delta p' \tag{11}$$

In all runs, we kept Poisson's ratio constant (0.25), and we discuss this assumption no further here. This does not mean that flow is independent of Poisson's ratio (Poliakov et al., 1993), but reflects the observation that Poisson's ratio does not vary significantly within the lower lithosphere.

We assume (and analyze) harmonic perturbations to the base of the layer (Fig. 1B):

$$\Delta h \cos kx, \text{ or } \Delta h' \cos k'x' \tag{12}$$

where $k=2\pi\ \lambda$ is wavenumber, and λ is wavelength. Thus, we restrict attention to two dimensions. Moreover, we assume that the lower layer is inviscid and inelastic, so as to mimic a large viscosity contrast between the unstable layer and the underlying layer. To test whether numerical instabilities might occur, we used widths of layers that were twice the wavelength of the perturbation, so that with reflecting side boundary conditions, downwelling sheets developed on the edges of the layer and in the middle. In all cases reported, we found no discernable difference between positions of the downwelling sheets on the margins and in the center.

Although we describe results with non-dimensional quantities, all runs were made using dimensionalized quantities. In all cases, h=100 km, g=9.8 m/s^2, ρ=3.3×10^3 kg/m^3, and $\Delta\rho$=100 kg/m^3. Fig. 2 shows the reference experiment for the case with viscosity of 5×10^{19} Pa s, μ=30 GPa and with a slippery top upper boundary condition. We then tested the influence of three different top boundary conditions (Fig. 3): (1) no slip and no vertical component of velocity (rigid top), (2) no shear stress and hence free horizontal slip, but no vertical movement (slippery top), and (3) for runs only with λ'=5, neither shear nor normal stress on the top boundary and hence free vertical and horizontal components of velocity and displacement (stress-free top). As shown in Figs. 2 and 3, the initially harmonic perturbation rapidly distorts into narrow downwelling drop-like plumes and broad regions of thinning. Moreover, as shown in Fig. 3, a slippery-top or stress-free boundary allows much more horizontal flow and thus greater thinning of the layer between downwelling sheets, and more rapid growth of the instability, than a rigid top. Because of the similarity of flow for slippery-top or stress-free boundaries, we discuss runs with stress-free top boundary no further.

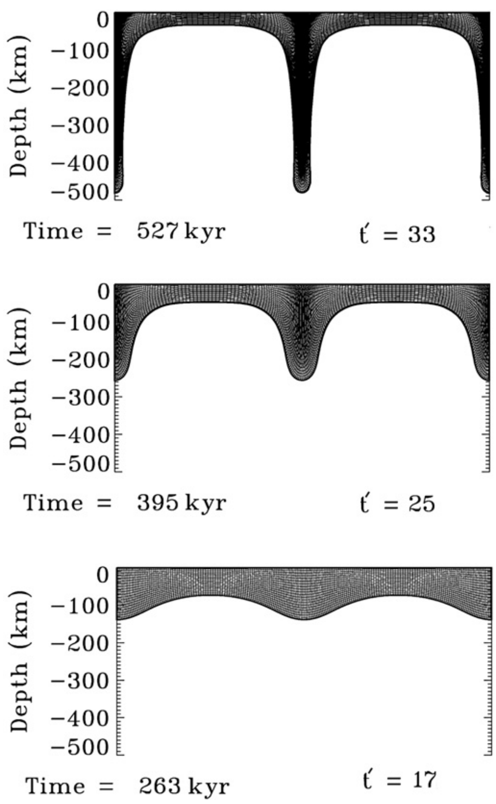

Fig. 2. Examples of an experimental run for the case with viscosity of 5×10^{19} Pa s and with a slippery top upper boundary condition, sampled at different times.

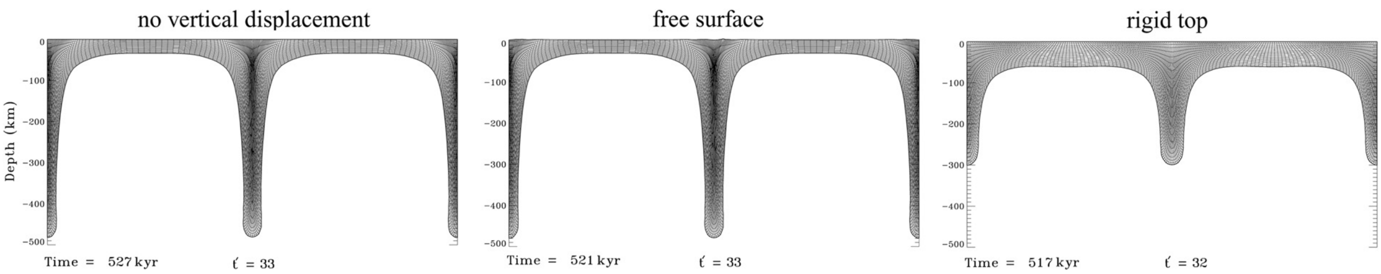

Fig. 3. Cross sections of the layer after approximately the same elapsed time of ~510,000 years (or dimensionless times of ~32), for runs with different top boundary conditions: a slippery top (left), free slip at the top (center), and a rigid top. There is no significant difference between the results for the first two conditions, but a rigid top boundary condition imposes slower growth rate.

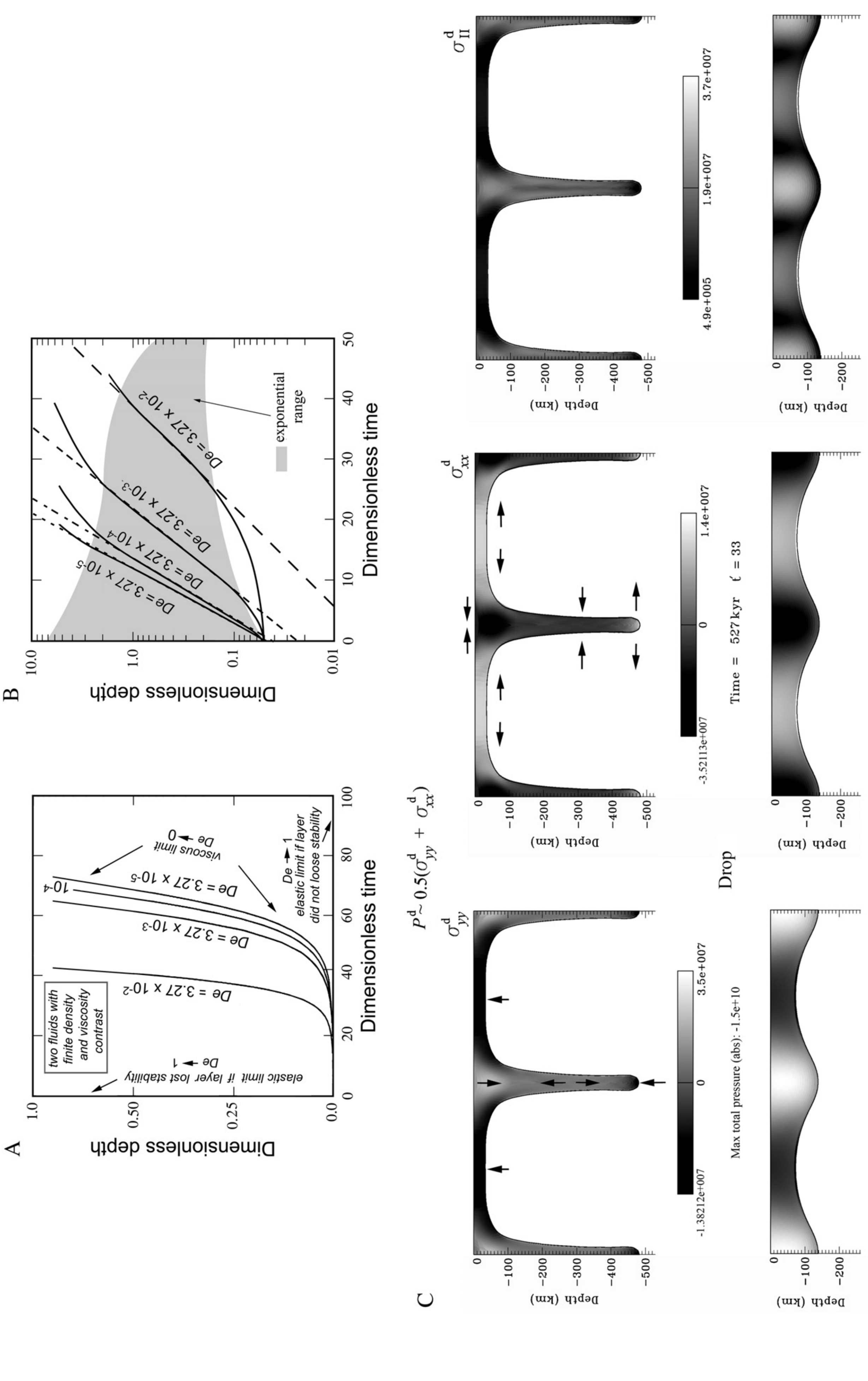
A
Dimensionless depth
Dimensionless time
two fluids with finite density and viscosity contrast
elastic limit if layer lost stability De → 1
De = 3.27 x 10-2
De = 3.27 x 10-3
10-4
De = 3.27 x 10-5
viscous limit De → 0
De → 1 elastic limit if layer did not loose stability
B
exponential range
C
Drop
Biot
Depth (km)
Time = 527 kyr t′ = 33
Time = 263 kyr t′ = 17
Max total pressure (abs): -1.5e+10
Max total pressure (abs): -4.35e+9

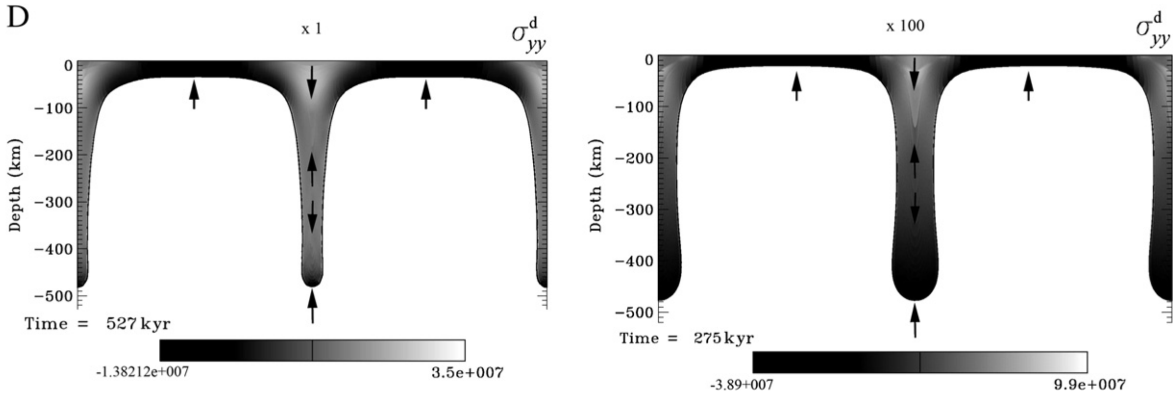

Fig. 4. A) Test of the numerical model on the previously treated case (Fig. 1B, case b) of two viscoelastic fluids with no or small viscosity contrast and identical elastic properties. It can be seen that in this case, the elasticity accelerates the growth of the instability in the same way as predicted by Poliakov et al. (1993) for finite viscosity contrasts and Biot (1965a,b) theory. B) Time series of displacements of downwelling sheets versus time. The logarithm of the maximum displacement of the downgoing sheet, normalized by layer thickness, $\log_{10} Z' = \log_{10} (Z/d)$, versus dimensionless time, $t' = t\,\Delta\rho gh/\eta$; thus exponential growth should plot as a straight line. In all cases, $k' = 1.257$, or $\lambda' = 5.0$. Note that for large values of the Deborah number $De = \Delta\rho gh/\mu$, corresponding to small values of elastic constants, initial growth is not exponential, but for small values of De, it is exponential for nearly the entire development of the instability. In all cases, at large descent distance, growth decelerates from exponential. Grey zone corresponds to exponential growth. C) Stress distributions for the experiments shown in Fig. 2. Transition from "Biot's" regime (bottom) to the "drop" regime is characterized by amplitudes of the deflected layer, W, exceeding h, and by relative increase of tensional component of the deviatoric stress σ^{d}_{yy}. The increase in σ^{d}_{y} refers to effective stretching of the drop filament. In this experiment, the deviatory stresses remain largely smaller than $\Delta\rho gh$. D) Comparison of the case with "normal" elastic modules $\mu = \lambda = 30$ GPa (left, experiment of Fig. 2) and 100 times higher elastic modules $\mu = = 3000$ GPa. Note higher growth rate in the latter case and radically different geometry of the drop head, filament and source layer.

To test the method used to solve the equations, we then ran a set of experiments (Fig. 4A) to compare with the previous results of Poliakov et al. (1993) for two-layer system with small viscosity contrast. We replaced the inviscid substratum and Winkler's boundary condition with a second viscoelastic layer of thickness $3h$, with the same elastic parameters as in the overlying layer, and with density $(\rho - \Delta\rho)$. These calculations match those of Poliakov et al. (1993). In particular, they confirm that for amplitudes of instability $<h$, limited viscosity ratios $<10^4$, and relatively high $De \geq 10^{-3}$, decreasing De results in higher growth rate than in case of pure viscous instability. In addition, these experiments show that for these conditions, the maximum accelerating effect of elasticity is reached for the smallest viscosity ratios, but the growth rate also decreases with increasing viscosity contrast so that the accelerating effect of elasticity becomes small for viscosity ratios $>10^6$. As predicted, the experiments of Fig. 4A confirm that in case when the surrounding fluid has a finite viscosity and same elastic modulus as the "drop," the stretching of the unstable layer is resisted by the surrounding fluid, and the behavior of the instability does not differ much from that predicted from Biot's theory.

In the next series of experiments we tested the influence of elasticity and viscosity on the growth rate of instability of a viscoelastic layer overlying an inviscid substratum with no elasticity (and hence infinite viscosity and elasticity contrasts). As follows from Eq. (3b) and confirmed by Poliakov et al. (1993) and the results shown in Fig. 4A, for sufficiently large De, for smaller elastic moduli, growth rates should increase. The degree to which elasticity, quantified by De, accelerates growth, however, depends on the boundary conditions which are quantified by value of the dimensionless constant r in (3b). To examine the effect of elasticity, we explored four values of μ, the shear modulus in the layer: 3×10^9 Pa, 3×10^{10} Pa, 3×10^{11} Pa, and 3×10^{12} Pa, for which values of De were 3.27×10^{-2}, 3.27×10^{-3}, 3.27×10^{-4}, and 3.27×10^{-5}. We carried out suites of runs with $\eta = 5\times10^n$, with $n = 18$, 19, 20, and 21 (Fig. 4B). In nearly all runs, we assumed for amplitudes of initial perturbation $\Delta h = 5$ km ($\Delta h' = 0.05$), but we also used $\Delta h = 1$ km ($\Delta h' = 0.01$) to examine whether the magnitude of the initial perturbation affected the development of the instability. It did not. We explored a spectrum of wavelengths of perturbations: 125, 187.5, 250, 375, 500, and 1000 km ($\lambda' = 1.25$, 1.875, 2.5, 3.75, 5, and 10) corresponding to $k' = kh = 5.0265$, 3.3510, 2.5133, 1.6755, 1.2566, and 0.62830, respectively. Thus, with as many as four values of η, for most wavenumbers of perturbation and each value of De, we obtained 4 values of the dimensionless growth rate.

4. Qualitative description of results and heuristic interpretation

With a small perturbation to the base of the layer, the thickened region sinks, and the thinned region thins (Figs. 2 and 3). The pattern of growth differs markedly for different values of De, which we implemented using different values of the shear modulus.

We may examine that growth by plotting the logarithm of the maximum (dimensionless) downward displacement of the sinking sheet ($log_{10}Z'$) versus (dimensionless) time t' (Fig. 4B). Analysis of linear stability (e.g., Chandrasekhar, 1961; Conrad and Molnar, 1997) shows that for viscous layer, growth is exponential, and hence a plot like that in Fig. 4B should yield a straight line, at least until non-linear interactions affect flow. Although linear stability applies only to small perturbations and small strains, numerical experiments using viscous layers confirm such a pattern until perturbations to the thickness of the layer exceed at least 10% of the layer thickness and as much as 100% for the fastest growing wavelength (e.g., Houseman and Molnar, 1997).

For purely viscous layers, growth accelerates to become super-exponential, and theoretically the sinking sheet would drop to an infinite depth in a finite time (e.g., Canright and Morris, 1993). Super-exponential growth is also expected in viscoelastic fluids with finite viscosity ratios, where increasing De would result in faster growth rates of instability, for amplitudes <100% of the layer thickness (Biot, 1965a,b). This growth to infinite depth, however, should not occur for a viscoelastic fluid, because the rapidly increasing strain rate should generate increasing elastic resistance to deformation, which marks the transition from "Biot's" mode to the "drop" mode (Fig. 4C). Indeed, Fig. 4C demonstrates that for large amplitudes of the deflected layer, $W>h$, there is a relative increase of the absolute value of the deviatoric stress component $\sigma^{d}yy$. The growth of $\sigma^{d}yy$ reflects the effective stretching of the drop filament.

Finally, Fig. 4D compares the case of $\mu = \lambda = 30$ GPa with the case where μ and λ are 100 times higher, for the same amplitude of the instability. As can be seen, the geometry of the drop head and filament are radically different, with a much thinner filament and smaller drop head in case of smaller elastic modules (See Appendix B). This explains why the growth rate is smaller for smaller elastic modules (smaller drop head → smaller driving force, thinner filament → higher internal shear and greater resistance to flow, as well as a smaller rate that fluid is drawn from the source layer). This figure also shows how the descent of the drop should eventually stall, as the source layer becomes vanishingly thin.

We may conclude that the inclusion of finite elasticity, to make the constitutive law viscoelastic, alters growth in two obvious ways, by delaying the onset of exponential growth and by altering the exponential growth rate so that super-exponential growth is virtually eliminated. For a viscoelastic layer, the growth of the instability, particularly for a small shear modulus, or large *De*, is delayed, so that exponential growth does not occur immediately. After relaxation ($t_M=\eta/\mu$) of the initial elastically induced stress, the growth of the developing instability may be retarded if elastic deformation (low μ or high *De*) continues to accommodate a significant fraction of the strain.

After a period of exponential growth, the growth of perturbations to viscous layers accelerates faster than exponential growth, but for viscoelasticity, the rate of exponential growth either stays nearly constant or in some cases decreases. This occurs because at this stage elastic strain in the filament becomes so large that the increasing elastic resistance retards deformation. We could not run calculations to times when a terminal speed was reached, but the deviation from exponential growth suggests that such a terminal speed might be approached (Fig. 4B). For large *De*, and hence small shear modulus with other parameters held fixed, elastic strain is large, and the deviation from exponential growth occurs at relatively small descent of the sheet. Thus, for large *De*, the duration of exponential growth is reduced both in the initial and final stages of growth. A widely observed example of this effect at small scale is a stalling of the growth of water drops due to quasi-elastic surface tension. A similar effect is observed in laboratory experiments of silicone drops that are devoid of surface tension but obey a viscoelastic rheology: initial retardation in the development of the instability, followed by acceleration (as in Biot's mode), and then a reduction of the growth rate when the layer is stretched and thinned, and its effective viscosity starts to increase giving rise to the drop mode (e.g., Smolka and Belmonte, 2003: Appendix B).

5. Results

To quantify the development of the instability, we measured growth rates, slopes of plots $\log_{10} Z'$ versus t', for the intervals over which growth is exponential (Fig. 4B). For small *De*, corresponding to large elastic moduli, growth is exponential for essentially the entire duration of runs, until the downwelling plumes reach 3–5 times the layer thickness (Fig. 4B). For large *De*, when elasticity starts to play role, however, exponential growth both is slower than for small *De* and applies for a smaller range of depths of descent. Note that by estimating a growth rate as we do, we obtain the largest average value of the growth rate, for we fit the linear portion of log_{10} Z′ versus t' through the point of inflection in such a plot. Because of the initial slow growth for runs with the largest value of *De*, estimated growth rates are more uncertain than for runs with smaller values of *De*, but as shown in the example in Fig. 5, the value of q' for large *De* cannot be as large as that for small *De*.

As expected, q' depends not only on *De*, but also on dimensionless wavenumber, k' (Fig. 5). For large wavenumber, growth rates for both free-slip and no-slip top boundaries decrease with increasing wave number, as is the case for viscous layers. For $k'=3.35$ or 5.03, only for the largest values of *De* are growth rates significantly different from those of a viscous layer (e.g., Conrad and Molnar, 1997; Houseman and Molnar, 1997).

For small k', growth rates for viscous layers are small for rigid top boundaries, but approach a maximum for free slip as $k' \rightarrow 0$. For viscoelastic layers, growth rates for relatively large values of *De* differ little from those for a viscous layer, but again growth is slower for smaller values of *De* (Fig. 5). Perhaps most interesting is the case of a free top, for which growth rates for large *De* are two to three times smaller than those for small *De*. In particular, for the largest value of *De* that we considered (3.27×10^{-2}), growth rates for small k' for rigid and free top boundaries differ little. Thus, for a wide range of values of *De*, the effect of the elastic component of viscoelasticity is small, but for sufficiently compliant material, scaled by the driving force due to buoyancy, the elastic component of strain can retard growth significantly and suppress growth of long-wavelength perturbations. This conclusion applies to the case of infinite viscosity contrasts and large deflection of the layer, as elasticity accelerates the growth of the instability otherwise.

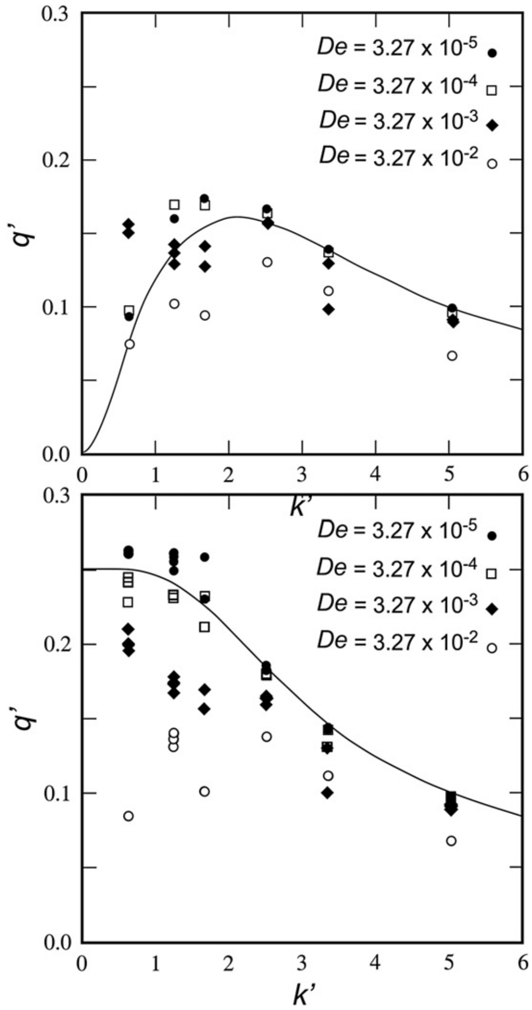

Fig. 5. Plots of dimensionless growth rates, q', versus dimensionless wave numbers, k', for different values of elastic constants, or different values of *De*, for no-slip top boundaries (a) and free-slip top boundaries (b). The solid lines show the theoretical predictions for the wave number dependence in a purely viscous layer with constant properties overlying an inviscid fluid (e.g., Conrad and Molnar, 1997). Note that viscoelastic layers follow the theoretical curve for large wave numbers, but grow faster at small wave numbers. Black symbols indicate runs with free slip permitted on the top boundary.

6. Discussion and conclusions

Most tectonically relevant scenarios refer to viscoelastic behavior with $De<10^{-4}$, or at most 10^{-3}. The effect of elasticity on the growth rate of Rayleigh–Taylor instability in such media is relatively small. The behavior of elastically compressible viscoelastic fluids with relatively low *De* ($<10^{-3}$) and very high material contrasts, conditions to which Biot's theory for incompressible viscoelastic fluids does not apply, may appear at tectonic scales, specifically for large deflections of an unstable layer. For layered media with very high viscosity and relaxation time ratios ($>10^6$), unlike the case of small ratios ($\sim10^2$–10^3), the inclusion of elasticity in a compressible formulation of the constitutive law relating stress to strain and strain rate can retard the initial and terminal growth of Rayleigh–Taylor instability, and therefore of convective instability. The effect of large deflection is similar to that of higher Poisson's ratio for small-amplitude instabilities, with the difference that the compressibility of the viscoelastic drop results in slower growth of instability for smaller shear modulus. If the unstable layer is underlain by a fluid with comparable viscosity and elastic moduli (Fig. 4A), however, that underlying fluid retards the stretching of the drop filament, and the behavior of the instability does not much differ from that predicted from Biot's theory.

For relatively stiff layers, the delay before exponential growth begins is short, and initial growth rates agree closely with those for purely viscous layers. For especially compliant layers, however, initially a perturbation to the thickness of the layer grows slowly, not exponentially: then when growth does increase exponentially with time it does so with a growth rate that is smaller than that for a purely viscous layer. The most marked difference between elastically stiff and compliant layers occurs for stress-free or slippery top boundaries: for viscous layers growth is fastest for perturbations with wavelengths that are long compared to the thickness of the layer, but for compliant layers, elasticity retards growth at long wavelengths, so that the layer behaves as if movement of its top surface were inhibited.

The calculations summarized above were made with the goal of spanning the likely range of parameters applicable to the earth. The applicable density anomalies $\Delta\rho$ are due to temperature anomalies ΔT in the mantle perhaps augmented by dense eclogitic lower crust. With a temperature at the Moho of 650 °C, for instance, and that for the asthenosphere of 1350 °C, a sensible maximum difference is 700 °C. The density anomaly due to thermal differences is given by $\Delta\rho=\rho\alpha\Delta T$, where $\rho\approx 3.3\times10^3$ kg m^{-3} is the background density of the mantle and $\alpha=3\times10^{-5}$ °C^{-1} is the coefficient of thermal expansion. Thus the maximum density anomaly will be 70 kg m^{-3}, and because the temperature gradient through the mantle lithosphere is essentially linear, the average density difference would be 35 kg m^{-3}. With a typical shear modulus of 7×10^{10} Pa for the mantle and assuming a layer thickness of 100 km, we obtain for mantle lithosphere $De=5\times10^{-4}$, which is relatively small among the values that we examined. Thus, we conclude that although elasticity will retard the growth of Rayleigh–Taylor and probably convective instability, the retarding effect should be small for normal lithosphere associated with large density contrasts ($h=100$ km, $\Delta\rho=35$ kg m^{-3}) and with an average viscosity $<10^{24}$ Pa s. This inference would not be the case if De were larger, for instance by 3 to 10 times, due either to thicker lithosphere or to larger density anomalies.

Archean lithosphere, which can be as thick as 250 km (or perhaps more) might be a candidate for large De, but the large lithospheric thickness is compensated by its relatively low density (e.g. Jordan, 1975). Thus, expected values of De for such regions ought not be much larger than 5×10^{-4}.

Elasticity seems likely to have its greatest effect in regions where normal lithosphere has thickened and where a thick eclogitic lower crust contributes to the density anomaly. For instance, Garzione et al. (2006) and Ghosh et al. (2006) showed that 3 ± 0.5 km of rapid surface uplift of the Altiplano and Central Andes between 10 and 6 Ma requires removal of eclogite-rich mantle lithosphere. Garzione et al. (2006) estimated that $\Delta\rho gh=8.1\times10^7$ Pa, and therefore $De=3\times10^{-3}$. Thus, elasticity could have helped stabilize lithosphere in that region and later retarded removal of it.

Finally, it may be suggested that in case of finite material contrasts (e.g. viscosity ratios$<10^5$), the development of the instability may be multi-stage: following Biot's theory in the initial stages (elasticity accelerates the growth rate) and then developing into the drop mode at the later stages, so that elasticity retards further growth. For small material contrasts, Biot's mode will likely prevail in most situations.

Acknowledgments

This research was begun while one of us (PM) was a guest of the Laboratoire de Tectonique, Université de Paris VI. It was supported in part by BRGM (Bureau des Recherches Géologiques et Minières), Dyeti/INSU and by the National Science Foundation through grant EAR-0337509, and a first draft was completed while PM was supported by the Miller Institute of Basic Research in Science at the University of California, Berkeley. We specially thank S. Babeyko and two anonymous reviewers for his very helpful comments. We also thank B. Kaus, M. Billen, P. van Keken, and L. Le Pourhiet for constructive criticism of an earlier draft of the manuscript.

Appendix A. Small-amplitude instabilities at low material contrasts: Biot's theory and other approximations

A.1. Biot's theory for small amplitudes

Biot (1965a,b), Biot and Odé (1962, 1965) and Odé (1966) used an analytical shear flow approximation, in which there are two or more "thick" layers of contrasting finite viscosity. The term "thick" here means that the upper and lower boundaries of the layer cannot be considered as parallel, and that the wavelength of the layer deflection cannot be considered large compared to its thickness. Biot's theory is based on an approximation for quasi-static incompressible viscous flow with constant.

Newtonian viscosity with in each layer, for which the Navier–Stokes equation can be written as:

$$\rho\frac{Du}{Dt}=\rho g_i-\frac{\partial P_d}{\partial x_i}+\eta\frac{\partial}{\partial x_j}\left(\dot{\varepsilon}_{ij}-\frac{1}{3}\dot{\varepsilon}_{ii}\delta_{ij}\right)\text{ with }\dot{\varepsilon}_{ii}=0\text{ and }\frac{Du}{Dt}=0 \tag{A1}$$

$$\sigma_{ij}=-P\delta_{ij}+\eta\left(\frac{\partial u_i}{\partial x_j}+\frac{\partial u_j}{\partial x_i}\right). \tag{A2}$$

Under this approximation, from continuity and incompressibility, the absolute values of normal stresses within each layer must be equal to each other:

$$\dot{\varepsilon}_{xx}+\dot{\varepsilon}_{yy}=0\Rightarrow\sigma_{xx}=-\sigma_{yy}\sim\eta\frac{\partial w}{\partial y} \tag{A3}$$

Pressure is eliminated by differentiation of the flow equation (A1), which is reduced to a fourth order (bi-harmonic) equation of the stream function $\psi\left(u_i=\frac{\partial\psi}{\partial x_j}\right)$, the unknown variable. The fourth-order characteristic equation has four roots, some of which, depending on the boundary and initial conditions and geometry of the problem, may be positive (growing) or negative (decaying). For positive roots, assuming a two-layered fluid system with no elasticity contrast, one obtains Eq. (3b) (Poliakov et al., 1993). Biot and Odé's (1962, 1965) and Odé's (1966) theory also treats only the positive roots (growing solution) of the problem.

Under this assumption, they showed that the geometry and boundary conditions have a crucial impact on the growth rate of instability. They considered a free-surface or rigid- surface at the top of a viscous layer of thickness h_1, viscosity η_1, and density ρ_1 overlying another viscous layer of finite thickness h_2, viscosity, η_2, and density ρ_2, for which the growth factor p depends on all of h_1, h_2, η_1, and η_2:

$$p=\frac{\Delta\rho g h_2}{\eta_1 r} \tag{A4}$$

The dependence on h_1 and η_2 is defined via the constants a, b, c in the characteristic stability equation $ar^2+br+c=0$. In particular, the minimal value of r decreases with increasing viscosity ratio: $r_{min}\approx 8$–12 for viscosity ratio 1, and $r_{min}\approx 0$–3 for viscosity ratio of 10^3. Varying h_2 has an inverse effect, since for a vertically infinite lower layer, and a free surface on the upper layer, r approaches infinity (but p remains finite). We note that the solutions of Biot (1965a,b) and Poliakov et al.

(1993) may not hold for Deborah numbers $De > 1$ (see Eq. (3b)) and for high viscosity ratios ($>10^3$), because this could lead to infinite growth rate. Indeed, Biot's (1965a,b; Kaus and Becker, 2007; Poliakov et al., 1993) solutions do not apply to large amplitudes and to large elasticity or viscosity contrasts, where viscoelastic drop theory becomes more applicable. In particular, Biot (1965a,b) has assumed that, by the correspondence principle, the effective viscosity of a layered media equals $\eta_{eff}=(\eta_1\eta_2)^{1/2}$. This assumption cannot apply to the case when η_2 is zero (infinite viscosity ratio), as the predicted growth rate would be zero for any layer overlying an inviscid fluid, which is incorrect.

A.2. Layer approximations

Biot's theory assumes that the viscoelastic stress cannot exceed $\Delta\rho gh$. Bending stresses in the deforming layer, however, may become significantly larger than $\Delta\rho gh$, and may provoke various kinds of instabilities in a viscoelastic medium. For example, for a thin, purely viscous layer, the bending deviatoric stress $\sigma^d_{xx}(y)$ and maximum bending stress $\sigma^d_{xx\max}$ are (Nadai, 1963):

$$\sigma^d_{xx}(y) = -2\eta\, y\frac{\partial^3 W}{\partial x^2 \partial t} \Rightarrow \sigma^d_{xx\max} = -\eta h\frac{\partial^3 W}{\partial x^2 \partial t} = -\eta h\frac{\partial^2 w}{\partial x^2} \tag{A5}$$

For a purely elastic layer, the maximum bending stress (Timoshenko and Young, 1968) is:

$$\sigma^d_{xx}(y) = \frac{E}{(1-\nu^2)}\, y\frac{\partial^2 W}{\partial x^2} \Rightarrow \sigma^d_{xx\max}\frac{E}{(1-\nu^2)}\frac{h}{2}\frac{\partial^2 W}{\partial x^2} \tag{A6}$$

where W is the vertical deflection of the layer, y is vertical distance from the middle of the layer, w is the deflection rate, E is Young's modulus, and ν is Poisson's ratio. Thus, for typical geological strain rates, $\dot\varepsilon$, of 10^{-13}–10^{-15} s^{-1} and viscosities of 10^{18}–10^{21} Pa s, viscous bending stresses may reach 10^8–10^{11} Pa, which are larger than simple viscous flow stresses $\eta\dot\varepsilon$ ($\eta\dot\varepsilon \sim 10^3$–$10^8$ Pa). The scale for the applied stress due to gravity, $\Delta\rho gh$, is on the order of 5×10^8 Pa and smaller than the maximum elastically supported bending stress. Indeed, in most cases related to the Earth: $\frac{1}{10h} \le \left|\frac{\partial^2 W}{\partial x^2}\right| \le \frac{1}{3h}$ (e.g., Watts and Burov, 2003). Consequently, for $h\sim100$ km, the maximum elastic bending stress is on the order of 10^8–10^{10} Pa and thus may exceed $\Delta\rho gh$ by several times.

Nadai (1963) considered relaxation under normal loading/unloading and horizontal compression of a single thin viscoelastic layer with a free upper surface over an inviscid layer with no elastic strength. He decomposed the total vertical deflection of the layer, W, into a reversible, or elastic deflection, W_e, and a permanent, or viscous deflection W_v such that $W=W_e+W_v$. For the decaying part of the solution corresponding to static flexure (negative roots of the characteristic equation), Nadai (1963) obtained:

$$W_v = \frac{e^{-t/t_M}}{t_M}\int_0^t We^{t/t_M}dt$$

$$W_e = W - W_v$$

or:

$$w = W_e/t_M$$
$$W_V = W_V(t=0) + \frac{1}{t_M}\int_0^t W_e dt \tag{A7b}$$

For a stable layer (Nadai, 1963), the deflection rate w caused by normal load P is proportional to $w\sim\frac{P}{\Delta\rho g}\int_0^\infty b(\lambda)\left(\left(c(\lambda)\frac{t_M}{(k(\lambda)D^4+m(\lambda))}-1\right)e^{-t/t_M}+1\right)\cos\lambda x d\lambda$ where $D = Eh^3/12(1-\upsilon^2)$ is elastic contribution to the flexural rigidity, and b, c, k, and m depend on layer geometry, boundary conditions, and wavelength, λ. Nadai (1963) showed that the application of a finite normal load to a viscoelastic layer first produces an elastic deflection, which eventually grows into a finite permanent viscous deflection. A dense viscous layer, however, becomes gravitationally unstable with an initial growth rate proportional to e^{t/t_0}. For an unstable viscoelastic layer, the deflection rate w is obtained from the positive root of the characteristic equation and contains a term that scales as $\left(\frac{t_M}{k(\lambda)D^4}-1\right)e^{t/t_M}$ where the parameter k does not depend on material properties.

According to this solution, a decrease in E may increase w via increasing pre-exponential term, but may also decrease it via decreasing the exponential term.

Appendix B. Drop theory of a viscoelastic fluid

Smolka and Belmonte (2003; Smolka et al., 2004) described and analyzed growth of a drop and connecting filament, which lengthens during growth, using a first-order approximation in terms of spring-force equation (y is downward positive):

$$\begin{aligned}&\Delta\rho\frac{\partial^2\left(L(t)R_d^3(t)\right)}{\partial t^2} = \Delta\rho g R_d^3(t) - \frac{3}{4}\left(\sigma_{yy}(t)-\sigma_{rr}(t)\right)R_f^2(t)\\ &R = f(t,\mu,\eta,B,\Delta\rho\dots)\\ &L = f(t,R,\mu,\eta,B,\Delta p\dots)\end{aligned} \tag{B1}$$

Here $R_d(t)$, $L(t)$, and $R_f(t)$ are the drop radius, filament length, and filament radius, respectively, the second term on the right is the restoring force due to stretching of the filament, and the first term on the right is the weight of the drop head. In the quasi-static limit, (B1) becomes:

$$\frac{4}{3}\Delta\rho g R_d^3(t,L) = \left(\sigma_{yy}(t)-\sigma_{rr}(t)\right)R_f^2(t,L) \tag{B2}$$

(The radial component of viscoelastic stress σ_{rr} can be roughly approximated as σ_{xx} in a 2D case.) With V representing the volume of the filament, as L increases the filament radius $R_f\,(t)\sim(V/\pi L(t))^{1/2}$ decreases. The deviatoric extensional stress in the filament, σ_f, which cannot be less than $4/3g\Delta\rho\, R_d^3/R_f^2$ (the weight of the drop head divided by the cross sectional area of filament section, πR_f^2), increases in inverse proportion to R_f^2 and in direct proportion to L. σ_f may grow to be come as large as (or exceed) $\Delta\rho gh$, especially if one takes into account the weight of the filament.

Small elastic moduli will result in a relatively large compressibility of the filament, which, consequently, will produce a thinner filament (smaller R_f), smaller drop head (smaller R_d), and hence smaller effective mass $(4/3\Delta\rho\pi R_d^3)$ at the end of the filament than will develop for large elastic moduli. Thus, small elastic moduli may lead to relatively slow growth. The stretching of compressible drop filament results in an increase in the apparent viscosity (=stress/strain rate), which can be referred to as effective "strain hardening."

Smolka and Belmonte (2003) concluded that depending on De, elasticity may either accelerate or decelerate the growth rate of drop instability. Their spring-force equation gives only a first-order of approximation, as it does not account, for example, for interaction between the filament and source layer, or for the transition from small instability to the drop mode. It must be noted that at the laboratory scale, surface tension makes a major contribution to σ_{rr} and hence to the stability of the layer. Naturally, surface tension does not exist at tectonic scales, but in two-layered fluid systems, material contrasts between the fluids play a role similar to that of surface tension in mono-fluid laboratory experiments. Indeed, the resistance of surrounding fluids to drop development is given by Stokes's and buoyancy forces, which, like surface tension, are proportional to the area (and thus to R^2) of the sphere. Also, the tensional stresses are maximum on the surface of the drop (Eq.s (A5), (A6) assuming $r\sim y$). Laboratory experiments of viscoelastic drops demonstrate complex behavior: initial retardation in the development of the instability, followed by acceleration, and then a reduction of the growth rate when the layer is over-stretched, and its effective viscosity starts to increase (~ drop mode).

The finite thickness of the source layer limits the maximum amplitude of the instability and thus its terminal growth rate, $\partial L/\partial t = w\infty$. In this case, the Deborah number is not constant, and Sostarecz and Belmonte (2003) redefine it as:

$$De_{\mathrm{Drop}} = t_M w / R_d \approx -t_M \; w \; d^2W/dx^2 \; (\text{if } W \sim h) \tag{B3}$$

where R_d, the radius of the drop, is equal to $-(d^2W/dx^2)^{-1}$ at the beginning of drop formation, and w equals the deflection or stretching rate, $\partial L/\partial t$, when the viscoelastic drop develops. Decreasing the shear modulus results in increasing t_M but in decreasing d^2W/dx^2. Consequently, according to (B3), elasticity may either increase or decrease De_{Drop}.

For low values of the Deborah number defined by (2) and appropriate for the Earth's lithosphere ($De < 10^{-3}$), the overall behavior of the system approaches the viscous limit but still differs from Newtonian behavior. In this case, if the Maxwell time is relatively long, the perturbation of the layer interface may be damped faster than the instability can grow. For a small shear modulus, the relaxation time can be large, possibly large enough to prevent the growth of the instability. The decelerating effect of smaller shear modulus in case of viscoelastic drop should be most important when the drop is immersed in an inviscid fluid. For a surrounding fluid with finite viscosity and same elastic modulus as the "drop," the stretching of the filament would be hampered, and then the behavior of the instability ought not differ much from that predicted by Biot's theory.

References

Biot, M.A., 1965a. Mechanics of Incremental Deformations. John Wiley & Sons, New York.

Biot, M.A., 1965b. Theory of viscous buckling and gravity instability of multilayers with large deformation. Geol. Soc. Amer. Bull. 76, 371–378.

Biot, M.A., Odé, H., 1962. On the folding of viscoelastic medium with adhering layer under compressive initial stress. Quart. Appl. Math. 19, 351–355.

Biot, M.A., Odé, H., 1965. Theory of gravity instability with variable overburden and compaction. Geophysics 30, 213–227.

Bird, R.B., Armstrong, R.C., Hassager, O., 1987. Dynamics of Polymeric Liquids, vol. 1. Wiley.

Burov, E., Guillou-Frottier, L., 2005. The plume head continental lithosphere interaction using a tectonically realistic formulation for the lithosphere. Geophys. J. Int. 161, 469–490.

Burov, E.B., Lobkovsky, L.I., Cloetingh, S., Nikishin, A.M., 1993. Continental lithosphere folding in Central Asia (part II). Tectonophysics 226 (1–4), 73–87.

Canright, D., Morris, S., 1993. Buoyant instability of a viscous film over a passive fluid. J. Fluid Mech. 255, 340–372.

Chandrasekhar, S., 1961. Hydrodynamic and Hydromagnetic Stability. Oxford Univ., Oxford. 652 pp.

Conrad, C.P., Molnar, P., 1997. The growth of Rayleigh–Taylor-type instabilities in the lithosphere for various rheological and density structures. Geophys. J. Int. 129, 95–112.

Conrad, C.P., Molnar, P., 1999. Convective instability of a boundary layer with temperature- and strain-rate-dependent viscosity in terms of "available buoyancy". Geophysical Journal International 139, 51–68.

Cundall, P.A., 1989. Numerical experiments on localization in frictional materials. Ingenieur-Archiv. 59, 148–159.

Ducea, M.N., Saleeby, J.B., 1996. Buoyancy sources for a large, unrooted mountain range, the Sierra Nevada, California: evidence from xenolith thermobarometry. J. Geophys. Res. 101, 8229–8244.

Ducea, M., Saleeby, J., 1998. A case for delamination of the deep batholithic crust beneath the Sierra Nevada, California. Int. Geol. Rev. 40, 78–93.

Garzione, C.N., Molnar, P., Libarkin, J.C., MacFadden, B., 2006. Rapid Late Miocene rise of the Bolivian Altiplano: evidence for removal of mantle lithosphere. Earth Planet. Sci. Lett. 241, 543–556.

Ghosh, P., Garzione, C.N., Eiler, J.M., 2006. Rapid uplift of the Altiplano revealed through ^{13}C–^{18}O bonds in paleosol carbonates. Science 311, 511–515.

Houseman, G.A., Molnar, P., 1997. Gravitational (Rayleigh–Taylor) instability of a layer with non-linear viscosity and convective thinning of continental lithosphere. Geophys. J. Int. 128, 125–150.

Houseman, G.A., McKenzie, D.P., Molnar, P., 1981. Convective instability of a thickened boundary layer and its relevance for the thermal evolution of continental convergent belts. J. Geophys. Res. 86, 6115–6132.

Jones, C.H., Farmer, G.L., Unruh, J.R., 2004. Tectonics of Pliocene removal of lithosphere of the Sierra Nevada, California. Geol. Soc. Amer. Bull. 116, 1408–1422.

Jordan, T.H., 1975. The continental tectosphere. Rev. Geophys. Space Phys. 13, 1–12.

Kaus, B.J.P., Becker, T.W., 2007. Effects of elasticity on the Rayleigh–Taylor instability: implications for large-scale geodynamics. Geophys J. Int. 168, 843–862. doi:10.1111/j.1365-246X.2006.03201.x.

Kittel, C., 1986. Introduction to Solid State Physics, 6th edition. Wiley, New York.

Nadai, A., 1963. Theory of Flow and Fracture of Solids. McGraw-Hill, New York. 705 pp.

Odé, H. (1966), Gravitational instability of multilayered system of high viscosity, PhD Thesis, Verhandlingen der Koninklijke Nederlandse Akademie van Wetenschappen , Afrd Natuurkunde, Eeerste Reeks – Deel XXIV – No 1, N.V., Noord Hollandsche Uitgevers Maatschappij , Amsterdam, pp 95.

Poliakov, A.N.B., Cundall, P., Podladchilov, Y., Laykhovsky, V., 1993. An explicit inertial method for the simulation of visco-elastic flow: an evaluation of elastic effects on diapiric flow in two- or three-layers models. In: Stone, D.B., Runcorn, S.K. (Eds.), Flow and creep in the solar system: observations, modelling and theory. Dynamic Modelling and Flow in the Earth and Planet Series. Kluwer Academic Publishers, Holland, pp. 175–195.

Reiner, M., 1964. The Deborah number. Phys. Today 62 (January).

Smolka, L.B., Belmonte, A., 2003. Drop pinch-off and filament dynamics of wormlike micellar fluids. J. Non-Newton. Fluid Mech. 115, 1–25.

Smolka, L.B., Belmonte, A., Henderson, D.M., Witelski, T.P., 2004. Exact solution for the extensional flow of a viscoelastic filament. Eur. J. Appl. Math. 15, 679–712.

Sostarecz, M.C., Belmonte, A., 2003. Motion and shape of a viscoelastic drop falling through a viscous fluid. J. Fluid Mech. 497, 235–252.

Timoshenko, S., Young, D.H., 1968. Elements of Strength of Materials, 5th edition. Van Nostrand, Princeton, NJ, p. 377.

Watts, A.B., Burov, E., 2003. Lithospheric strength and its relationship to the elastic and seismogenic layer thickness. Earth Planet. Sci. Lett. 213, 113–131.

Whitehead Jr., J.A., Luther, D.S., 1975. Dynamics of laboratory diapir and plume models. J. Geophys. Res. 80, 705–717.